JACS
JOURNAL OF THE AMERICAN CHEMICAL SOCIETY
Communication
Cite This: J. Am. Chem. Soc. 2019, 141, 17989−17994
pubs.acs.org/JACS

Radical Dimerization in a Plastic Organic Crystal Leads to Structural and Magnetic Bistability with Wide Thermal Hysteresis

Alina Dragulescu-Andrasi,[†] Alexander S. Filatov,[‡] Richard T. Oakley,[§] Xiang Li,[†] Kristina Lekin,[§] Ashfia Huq,[∥] Chongin Pak,[†,○] Samuel M. Greer,[†,⊥,◆] Johannes McKay,[⊥] Minyoung Jo,[†] Jeff Lengyel,[†] Ivan Hung,[⊥] Elvis Maradzike,[†] A. Eugene DePrince, III,[†] Sebastian A. Stoian,[†,⊥,▽] Stephen Hill,[⊥,#] Yan-Yan Hu,[†,⊥] and Michael Shatruk*[,†,⊥]

[†]Department of Chemistry and Biochemistry, Florida State University, Tallahassee, Florida 32306, United States
[‡]Department of Chemistry, University of Chicago, Chicago, Illinois 32306, United States
[§]Department of Chemistry, University of Waterloo, Waterloo, Ontario N2L 3G1, Canada
[∥]Neutron Scattering Division, Oak Ridge National Laboratory, Oak Ridge, Tennessee 37831, United States
[⊥]National High Magnetic Field Laboratory, Tallahassee, Florida 32310, United States
[#]Department of Physics, Florida State University, Tallahassee, Florida 32306, United States

Supporting Information

ABSTRACT: The nitroxyl radical 1-methyl-2-azaadamantane *N*-oxyl (Me-AZADO) exhibits magnetic bistability arising from a radical/dimer interconversion. The transition from the rotationally disordered paramagnetic plastic crystal, Me-AZADO, to the ordered diamagnetic crystalline phase, $(Me\text{-}AZADO)_2$, has been conclusively demonstrated by crystal structure determination from high-resolution powder diffraction data and by solid-state NMR spectroscopy. The phase change is characterized by a wide thermal hysteresis with high sensitivity to even small applied pressures. The molecular dynamics of the phase transition from the plastic crystal to the conventional crystalline phase has been tracked by solid-state (^1H and ^{13}C) NMR and EPR spectroscopies.

Magnetically bistable molecular materials are appealing because of their synthetic tunability and light weight. They also serve as rich testbeds for theoretical approaches in condensed-matter physics. Examples of molecular magnetic bistability include order−disorder transitions in molecule-based magnets,[1−7] switching between two magnetic states of opposite spin orientation in single-molecule magnets,[8−18] conversion between the low-spin and high-spin electronic configurations in spin-crossover complexes,[19−28] and reversible dimerization of organic π radicals.[29−39] Despite the extensive research on these bistability phenomena, there remains sustained interest in uncovering new mechanisms that can be harnessed for the design of magnetically bistable systems. In this vein, recent discoveries of coordination-environment-dependent switching between two spin states of a transition metal complex in solution[40] and the light-induced cleavage of a σ dimer of organic radicals into a pair of π radicals in the solid state[41,42] leveraged the role of structural effects in promoting magnetic bistability.

Herein we demonstrate that plastic crystalline phases represent a new frontier in the design of bistable magnetic materials. Such phases are generally not accessible with the relatively large transition metal complexes or planar $\pi-\pi$-stacked organic radicals. As an intermediate phase between the liquid and solid states, plastic crystals have a low energy barrier to molecular rotation, which results in crystal structures with highly symmetric positional order but severe orientational disorder. In the plastic crystalline state, each molecule literally spins around its center of mass. Below a certain critical temperature, a phase transition to a regular ordered crystalline phase occurs. Small organic molecules have provided numerous examples of such behavior.[43,44] Exploring the rotational landscapes of light, purely organic spin-carrying radicals offers a unique approach to coupling the structural and magnetic phase transitions. Such magnetostructural transitions often lead to bistability in physical properties, which is manifested as irreversible (hysteretic) behavior observed in successive cooling−heating measurement cycles. For example, $\pi-\pi$-stacked organic radicals are well-known to undergo such transitions, generally known as Peierls dimerization.[45,46]

Among the organic compounds known to form plastic crystalline phases, adamantane stands out not only as one of the most studied molecules[47−50] but also as a parent structure to a class of nitroxyl radicals that includes 2-azaadamantane *N*-oxyl (AZADO) and 1-methyl-2-azaadamantane *N*-oxyl (Me-AZADO) (Chart 1). In contrast to many other promising organic radicals that incorporate heavier p-block heteroatoms

Chart 1

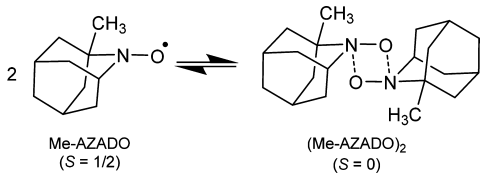

Received: September 3, 2019
Published: October 29, 2019

DOI: 10.1021/jacs.9b09533
J. Am. Chem. Soc. 2019, 141, 17989−17994

such as sulfur, these 2-azaadamantane-based radicals incorporate solely light-weight elements (C, H, O, and N) and are air-stable, allowing for convenient bench manipulation under ambient conditions.

Structural transitions associated with the dimerization of free radicals often result in dramatic color changes. For this reason, our attention was drawn to the batch-dependent color of the *N*-oxyl radical, Me-AZADO.[51] This radical is also thermochromic, as its color changes from red to yellow upon cooling. The red color is restored upon warming to room temperature. We hypothesized that the color change from red (specific to free *N*-oxyl radicals) to yellow is indicative of diminished radical character due to the formation of a diamagnetic dimer state. A comprehensive study of this compound, as reported below, revealed a remarkable phase transition with a wide thermal hysteresis that is pronounced in all of the physical and spectroscopic properties of Me-AZADO.

Variable-temperature magnetic susceptibility (χ) measurements performed under ambient pressure on a sample of Me-AZADO loosely packed in a polytetrafluoroethylene capsule revealed an abrupt transition from the paramagnetic ($S = {}^1/_2$) to diamagnetic ($S = 0$) state upon cooling below $T_\downarrow = 267$ K (Figure 1). Upon heating, the reverse transition occurred at the midpoint $T_\uparrow = 285$ K. Interestingly, we found that the hysteresis loop widened from 18 K to ~30 K when the sample was manually compressed in a standard polycarbonate capsule for magnetic measurements (Figure S1). Subsequently, in measurements under controlled pressure in a clamp cell, the hysteresis loop widened to 30 K at 700 bar ($T_\downarrow = 256$ K, $T_\uparrow = 286$ K) and to 35 K at 900 bar ($T_\downarrow = 250$ K, $T_\uparrow = 285$ K).[52] The change in the hysteresis width occurred solely as a result of the shift of the lower-temperature transition in the cooling mode, while the higher-temperature transition observed in the heating mode was much less affected by pressure (Figure 1).

The apparent temperature-driven phase transition in Me-AZADO was examined by differential scanning calorimetry (DSC). A sharp exothermic peak was observed at 240 K in the cooling mode, while a corresponding endothermic peak was observed at 285 K in the heating mode (Figure S2). Yet again, a large change in the hysteresis width was observed that was due to pressurization of the polycrystalline sample, which was tightly sealed in the aluminum pan used for the DSC measurements. A similar thermally induced transition with a hysteresis of ~20 K was observed earlier in the related AZADO radical, but neither pressure effects nor comprehensive characterization were reported for that compound.[53] Here we elucidate the nature of the strongly hysteretic phase transition in Me-AZADO by a combination of structural and spectroscopic methods.

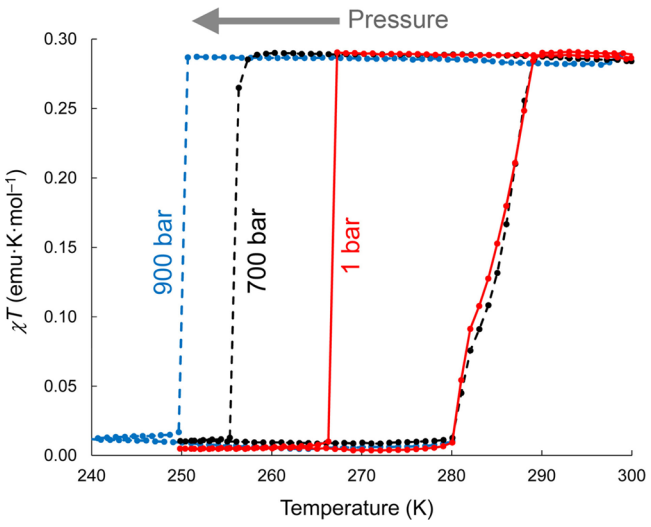

Figure 1. Temperature dependence of χT measured on a polycrystalline sample of Me-AZADO at different pressures. The cooling and heating rates were 0.5 K min^{-1}.

Attempts to determine the crystal structure of Me-AZADO by single-crystal X-ray diffraction using laboratory X-ray sources were thwarted by the extreme mechanical sensitivity (softness) of the crystals, as even gentle handling led to the loss of the single-crystal nature. The few crystals that were successfully mounted either sublimed under a weak flow of nitrogen gas or fractured upon cooling. This issue prompted the use of high-resolution powder X-ray diffraction (PXRD) provided by synchrotron radiation at the Advanced Photon Source (Argonne National Laboratory). The PXRD data sets were collected on a microcrystalline sample of Me-AZADO during stepwise cooling and reheating over the temperature range from 295 to 220 K. The obtained PXRD patterns confirmed the crystallinity of the sample and revealed dramatic changes as a function of temperature and sample history (Figure 2).

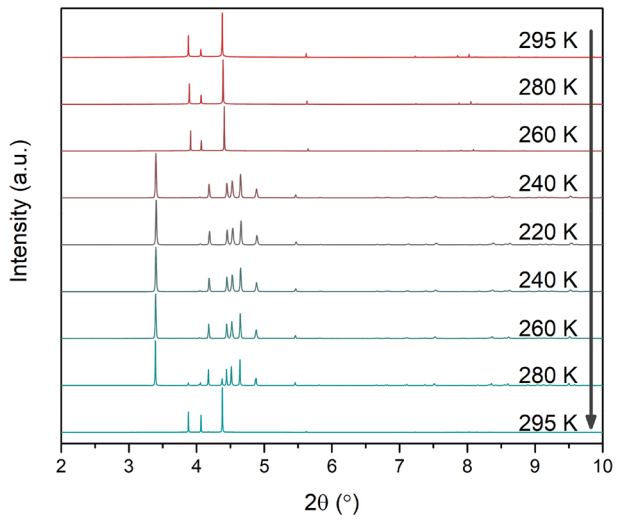

Figure 2. PXRD patterns for Me-AZADO collected upon cooling and subsequent reheating under synchrotron irradiation ($\lambda = 0.414561$ Å).

PXRD data sets collected on the plastic phase of Me-AZADO at 295, 280, and 260 K showed a few very sharp peaks that were indexed in the hexagonal space group $P6_3/m$ (see the top three patterns in Figure 2 and the unit cell parameters in Table S1). This result was not surprising; the observation of high space-group symmetry is well-established for plastic crystals, reflecting a high degree of rotational disorder.[54,55] On the basis of this premise, the 260 K diffraction pattern obtained in the cooling regime was successfully modeled by assuming sixfold disorder of the Me-AZADO radical about the 6_3 axis of the $P6_3/m$ space group (Figure 3a). While this solution represents only an approximation to the real structure of the plastic phase, it provides a useful framework for rationalizing the solid-state NMR measurements described below.

With continued cooling to 240 K, the PXRD pattern of Me-AZADO changed dramatically, heralding the radical-to-dimer

DOI: 10.1021/jacs.9b09533
J. Am. Chem. Soc. 2019, 141, 17989−17994

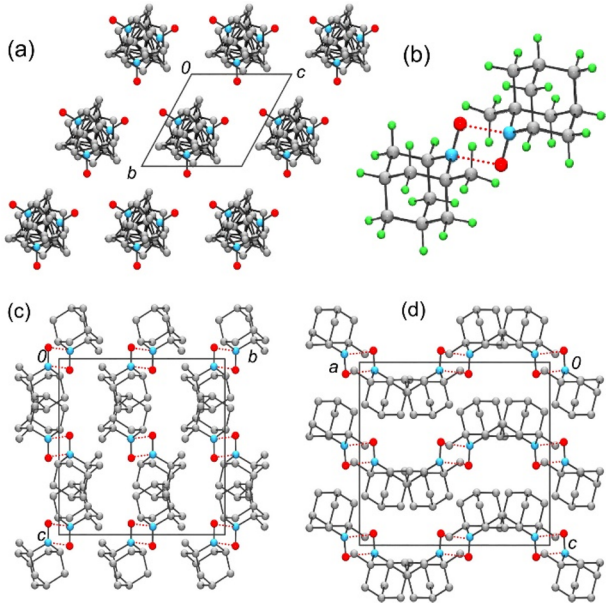

Figure 3. (a) Crystal structure of the $P6_3/m$ plastic phase of Me-AZADO at 260 K, showing the radicals disordered as pinwheels about the 6_3 axes. (b) Dimer unit in the *Pbca* phase at 260 K, with N···O′ intradimer contacts shown in red. (c, d) Crystal packing of dimers shown parallel to (c) the *a* axis and (d) the *b* axis in the *Pbca* phase. In the packing diagrams, H atoms have been omitted for clarity.

phase transition observed in the magnetic measurements. Initial attempts to index the 220 K data suggested a tetragonal unit cell, but no space group could be identified that afforded a sensible structural solution. Eventually, we considered the possibility of lower symmetry and found that the data could be indexed in the orthorhombic space group *Pbca* with nearly equal *b* and *c* unit cell parameters. The validity of this assignment was supported by subsequent data sets collected at 240, 260, and 280 K, which showed a small but consistent divergence in the relative lengths of the *b* and *c* axes (Figure S4) with increasing temperature. During the last of these collections, intruder peaks corresponding to ∼10% conversion back to the starting $P6_3/m$ phase were present (Figure 2).

For the data obtained after reheating to 260 K, a structural solution was pursued using simulated-annealing methods and a rigid-body restriction based on a starting model obtained from density functional theory (DFT) geometry optimization of a single Me-AZADO radical. The structure was refined by Rietveld methods (Figure S5), with atomic positions and isotropic atomic displacement parameters taken from the initial simulated annealing model; the final unit cell parameters and refinement quality indices are listed in Table S1. The dimer unit consists of a centrosymmetric pair of Me-AZADO radicals linked by short (2.51(6) Å) N···O′ intradimer interactions (Figure 3b). The crystal packing is shown in Figure 3c,d. The overall structure of the dimer was also in reasonable agreement with a model obtained by gas-phase DFT calculations (Figure S6), which showed an intradimer N···O′ distance of 2.28(6) Å. Essentially identical solutions were obtained using the 240 and 220 K data.

Variable-temperature neutron powder diffraction (NPD) was performed at Oak Ridge National Laboratory. The data were collected on a non-deuterated sample of Me-AZADO upon cooling from 300 to 10 K. The refined unit cell parameters showed that the *b* axis continued to contract more rapidly with temperature than the *c* axis, giving rise to an accidental equivalence in their values near 200 K (Figure S4). The evolution of the NPD patterns with temperature confirmed the abrupt structural phase transition (Figure S7a). The structure of the dimer obtained from the PXRD data was also successfully refined against the NPD data collected at 10 K (Figure S7b).

Magic-angle-spinning (MAS) solid-state ^{1}H NMR spectra recorded at 303 K revealed four major ^{1}H resonances at −48, −15, −2, and 2 ppm, attributable to four types of protons in Me-AZADO (Figures 4 and S8a). For the H4 protons, which are farthest away from the unpaired electron, the shift observed at 2.0 ppm is mainly from chemical shielding, which explains its similarity to the 1.8 ppm shift observed for the same type of protons in the diamagnetic analogue, 1-methyl-2-azaadamantan-2-ol (Me-AZADO-H) (Figure S9). For the H1 protons, which at four bonds away are the closest to the unpaired electron, the Fermi contact interaction between H1 and the unpaired electron shifts the resonance from 5 ppm to −48 ppm. A group of broad ^{1}H peaks observed between 5 and 10 ppm are attributed to the diamagnetic Me-AZADO-H impurity.

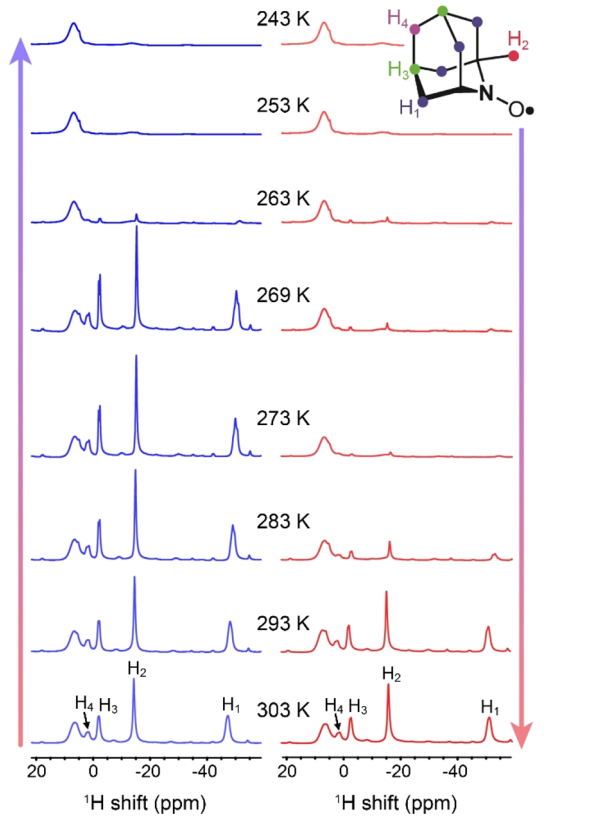

Figure 4. Solid-state ^{1}H NMR spectra for Me-AZADO collected upon cooling and subsequent reheating at 18.8 T (800 MHz for ^{1}H).

The 303 K ^{13}C NMR spectrum showed three major resonances at 255, −70, and 143 ppm, attributed to the C1, C2, and C3 atoms (Figure S8b), which appear two, three, and four bonds away from the unpaired electron, respectively. Although the methyl group carbon is clustered into the C1-type atoms, it is not chemically equivalent to the rest of the C1 atoms, which leads to the unresolved splitting of the resonance at 255 ppm. A cluster of broadened resonances at 80−140 ppm

DOI: 10.1021/jacs.9b09533
J. Am. Chem. Soc. 2019, 141, 17989−17994

was assigned to residual $(Me\text{-}AZADO)_2$ dimers, while the well-resolved resonances at 30−70 ppm are from the Me-AZADO-H impurity.

The dynamics of the phase transition was followed by the evolution of the ^1H resonances with temperature (Figure 5). During cooling from 303 to 269 K, only minor changes in the H1, H2, H3, and H4 resonances were observed, but all of these resonances abruptly disappeared below 269 K. This observation was initially surprising given that our magnetic and crystal structure data confirmed the formation of the diamagnetic $(Me\text{-}AZADO)_2$ dimers at lower temperatures.

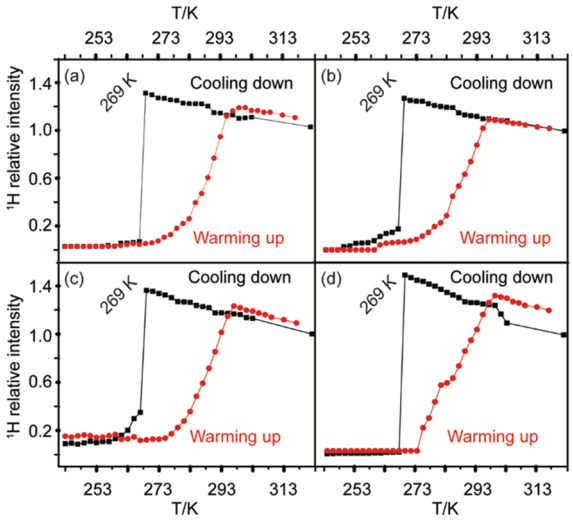

Figure 5. Temperature dependence of the relative intensities of the ^1H resonances for atoms (a) H1, (b) H2, (c) H3, and (d) H4.

Variable-temperature EPR spectra revealed that the intensity of the paramagnetic signal greatly diminished as the temperature was lowered (Figure S10) but did not disappear even at 4 K. This remnant signal results from molecules that are unable to link with neighboring sites during dimer formation and thus form radical defects in the dimer phase.[56] Analysis of the spectral intensity suggested that ∼5% of the paramagnetic species remained at low temperatures. Considering the arrest of molecular motion upon dimerization in the solid state, the residual nondimerized radicals form paramagnetic "islands" that broaden (wipe out) the NMR signal from the $(Me\text{-}AZADO)_2$ dimers. The NMR resonances reappear upon warming above 285 K, in accordance with the magnetic and structural data.

The strongly hysteretic magnetostructural phase transition stemming from the competition between the local rotational disorder in the plastic phase and the long-range order in the crystalline phase suggests that such an approach can be generalized for the discovery of new molecular systems with remarkable magnetic and structural bistability. We expect that our work will stimulate further research in this direction.

■ ASSOCIATED CONTENT

Supporting Information

The Supporting Information is available free of charge on the ACS Publications website at DOI: 10.1021/jacs.9b09533.

Description of materials and methods and additional magnetic, calorimetric, PXRD, MAS NMR, and EPR data (PDF)

Crystallographic data for Me-AZADO at 260 K (CIF)

Crystallographic data for $(Me\text{-}AZADO)_2$ at 260 K (CIF)

■ AUTHOR INFORMATION

Corresponding Author

*mshatruk@fsu.edu

ORCID

Alexander S. Filatov: 0000-0002-8378-1994
Richard T. Oakley: 0000-0002-7185-2580
Samuel M. Greer: 0000-0001-8225-3252
Jeff Lengyel: 0000-0002-5053-6263
A. Eugene DePrince, III: 0000-0003-1061-2521
Sebastian A. Stoian: 0000-0003-3362-7697
Stephen Hill: 0000-0001-6742-3620
Yan-Yan Hu: 0000-0003-0677-5897
Michael Shatruk: 0000-0002-2883-4694

Present Addresses

▽S.A.S.: Department of Chemistry, University of Idaho, 875 Perimeter Drive, Moscow, ID 83844.

○C.P.: Applied Superconductivity Center, National High Magnetic Field Laboratory, 1800 East Paul Dirac Drive, Tallahassee, FL 32310.

◆S.M.G.: Los Alamos National Laboratory, P.O. Box 1663, Los Alamos, NM 87545.

Notes

The authors declare no competing financial interest.

■ ACKNOWLEDGMENTS

This research was supported by the National Science Foundation (Awards CHE-1464955 to M.S., CHE-1554354 to A.E.D., and DMR-1610226 to S.H.). The NMR and EPR spectra were obtained at the National High Magnetic Field Laboratory, supported by NSF Cooperative Agreement DMR-1644779 and the State of Florida. Use of the Advanced Photon Source at Argonne National Laboratory was supported by the U.S. Department of Energy (DOE), Office of Science, Office of Basic Energy Sciences, under Contract DE-AC02-06CH11357. A portion of this research used resources at the Spallation Neutron Source, a DOE Office of Science User Facility operated by Oak Ridge National Laboratory.

■ REFERENCES

(1) Avendano, C.; Hilfiger, M. G.; Prosvirin, A.; Sanders, C.; Stepien, D.; Dunbar, K. R. Temperature and light induced bistability in a $Co_3[Os(CN)_6]_2{\cdot}6H_2O$ Prussian blue analog. *J. Am. Chem. Soc.* **2010**, *132*, 13123−13125.

(2) Ruiz, E.; Rodriguez-Fortea, A.; Alvarez, S.; Verdaguer, M. Is it possible to get high T_C magnets with Prussian blue analogues? A theoretical prospect. *Chem. - Eur. J.* **2005**, *11*, 2135−2144.

(3) Ohkoshi, S. i.; Hashimoto, K. Design of a novel magnet exhibiting photoinduced magnetic pole inversion based on molecular field theory. *J. Am. Chem. Soc.* **1999**, *121*, 10591−10597.

(4) Sato, O.; Iyoda, T.; Fujishima, A.; Hashimoto, K. Photoinduced magnetization of a cobalt-iron cyanide. *Science* **1996**, *272*, 704−705.

(5) Mallah, T.; Thiebaut, S.; Verdaguer, M.; Veillet, P. High-T_C molecular-based magnets: ferrimagnetic mixed-valence chromium(III)-chromium(II) cyanides with T_C at 240 and 190 K. *Science* **1993**, *262*, 1554−1557.

(6) Ferlay, S.; Mallah, T.; Ouahes, R.; Veillet, P.; Verdaguer, M. A room-temperature organometallic magnet based on Prussian blue. *Nature* **1995**, *378*, 701−703.

DOI: 10.1021/jacs.9b09533
J. Am. Chem. Soc. 2019, 141, 17989−17994

(7) Holmes, S. M.; Girolami, G. S. Sol-gel synthesis of $KV^{II}[Cr^{III}(CN)_6]\cdot 2H_2O$: a crystalline molecule-based magnet with a magnetic ordering temperature above 100°C. *J. Am. Chem. Soc.* **1999**, *121*, 5593−5594.
(8) Goodwin, C. A. P.; Ortu, F.; Reta, D.; Chilton, N. F.; Mills, D. P. Molecular magnetic hysteresis at 60 K in dysprosocenium. *Nature* **2017**, *548*, 439−442.
(9) Guo, F.-S.; Day, B. M.; Chen, Y.-C.; Tong, M.-L.; Mansikkamaeki, A.; Layfield, R. A. Magnetic hysteresis up to 80 K in a dysprosium metallocene single-molecule magnet. *Science* **2018**, *362*, 1400−1403.
(10) Godfrin, C.; Ferhat, A.; Ballou, R.; Klyatskaya, S.; Ruben, M.; Wernsdorfer, W.; Balestro, F. Operating quantum states in single magnetic molecules: implementation of Grover's quantum algorithm. *Phys. Rev. Lett.* **2017**, *119*, 187702.
(11) Thiele, S.; Balestro, F.; Ballou, R.; Klyatskaya, S.; Ruben, M.; Wernsdorfer, W. Electrically driven nuclear spin resonance in single-molecule magnets. *Science* **2014**, *344*, 1135−1138.
(12) Bogani, L.; Wernsdorfer, W. Molecular spintronics using single-molecule magnets. *Nat. Mater.* **2008**, *7*, 179−186.
(13) Ishikawa, N.; Sugita, M.; Wernsdorfer, W. Nuclear spin driven quantum tunneling of magnetization in a new lanthanide single-molecule magnet: bis(phthalocyaninato)holmium anion. *J. Am. Chem. Soc.* **2005**, *127*, 3650−3651.
(14) Wernsdorfer, W.; Aliaga-Alcalde, N.; Hendrickson, D. N.; Christou, G. Exchange-biased quantum tunnelling in a supramolecular dimer of single-molecule magnets. *Nature* **2002**, *416*, 406−409.
(15) Sessoli, R.; Gatteschi, D.; Caneschi, A.; Novak, M. A. Magnetic bistability in a metal-ion cluster. *Nature* **1993**, *365*, 141−143.
(16) Thomas, L.; Lionti, F.; Ballou, R.; Gatteschi, D.; Sessoli, R.; Barbara, B. Macroscopic quantum tunnelling of magnetization in a single crystal of nanomagnets. *Nature* **1996**, *383*, 145−147.
(17) Demir, S.; Gonzalez, M. I.; Darago, L. E.; Evans, W. J.; Long, J. R. Giant coercivity and high magnetic blocking temperatures for N_2^{3-} radical-bridged dilanthanide complexes upon ligand dissociation. *Nat. Commun.* **2017**, *8*, 2144.
(18) Rinehart, J. D.; Fang, M.; Evans, W. J.; Long, J. R. A N2(3-) radical-bridged terbium complex exhibiting magnetic hysteresis at 14 K. *J. Am. Chem. Soc.* **2011**, *133*, 14236−14239.
(19) Delgado, T.; Tissot, A.; Guénée, L.; Hauser, A.; Valverde-Muñoz, F. J.; Seredyuk, M.; Real, J. A.; Pillet, S.; Bendeif, E.-E.; Besnard, C. Very long-lived photogenerated high-spin phase of a multistable spin-crossover molecular material. *J. Am. Chem. Soc.* **2018**, *140*, 12870−12876.
(20) Liu, C.; Zhang, J.; Lawson Daku, L. M.; Gosztola, D.; Canton, S. E.; Zhang, X. Probing the impact of solvation on photoexcited spin crossover complexes with high-precision X-ray transient absorption spectroscopy. *J. Am. Chem. Soc.* **2017**, *139*, 17518−17524.
(21) Phan, H.; Benjamin, S. M.; Steven, E.; Brooks, J. S.; Shatruk, M. Photomagnetic response in highly conductive iron(II) spin-crossover complexes with TCNQ radicals. *Angew. Chem., Int. Ed.* **2015**, *54*, 823−827.
(22) Steinert, M.; Schneider, B.; Dechert, S.; Demeshko, S.; Meyer, F. A trinuclear defect-grid iron(II) spin crossover complex with a large hysteresis loop that is readily silenced by solvent vapor. *Angew. Chem., Int. Ed.* **2014**, *53*, 6135−6139.
(23) Koo, Y. S.; Galan-Mascaros, J. R. Spin crossover probes confer multistability to organic conducting polymers. *Adv. Mater.* **2014**, *26*, 6785−6789.
(24) Shepherd, H. J.; Gural'skiy, I. A.; Quintero, C. M.; Tricard, S.; Salmon, L.; Molnár, G.; Bousseksou, A. Molecular actuators driven by cooperative spin-state switching. *Nat. Commun.* **2013**, *4*, 2607.
(25) Ohkoshi, S. I.; Tokoro, H. Photomagnetism in cyano-bridged bimetal assemblies. *Acc. Chem. Res.* **2012**, *45*, 1749−1758.
(26) Li, F.; Clegg, J. K.; Goux-Capes, L.; Chastanet, G.; D'Alessandro, D. M.; Letard, J. F.; Kepert, C. J. A mixed-spin molecular square with a hybrid [2 × 2]grid/metallocyclic architecture. *Angew. Chem., Int. Ed.* **2011**, *50*, 2820−2823.
(27) Bressler, C.; Milne, C.; Pham, V. T.; ElNahhas, A.; van der Veen, R. M.; Gawelda, W.; Johnson, S.; Beaud, P.; Grolimund, D.; Kaiser, M.; Borca, C. N.; Ingold, G.; Abela, R.; Chergui, M. Femtosecond XANES study of the light-induced spin crossover dynamics in an iron(II) complex. *Science* **2009**, *323*, 489−492.
(28) Sato, O.; Tao, J.; Zhang, Y. Z. Control of magnetic properties through external stimuli. *Angew. Chem., Int. Ed.* **2007**, *46*, 2152−2187.
(29) Fujita, W.; Awaga, K. Room-temperature magnetic bistability in organic radical crystals. *Science* **1999**, *286*, 261−262.
(30) Lekin, K.; Winter, S. M.; Downie, L. E.; Bao, X. Z.; Tse, J. S.; Desgreniers, S.; Secco, R. A.; Dube, P. A.; Oakley, R. T. Hysteretic spin crossover between a bisdithiazolyl radical and its hypervalent σ-dimer. *J. Am. Chem. Soc.* **2010**, *132*, 16212−16224.
(31) Brusso, J. L.; Clements, O. P.; Haddon, R. C.; Itkis, M. E.; Leitch, A. A.; Oakley, R. T.; Reed, R. W.; Richardson, J. F. Bistabilities in 1,3,2-dithiazolyl radicals. *J. Am. Chem. Soc.* **2004**, *126*, 8256−8265.
(32) McManus, G. D.; Rawson, J. M.; Feeder, N.; van Duijn, J.; McInnes, E. J. L.; Novoa, J. J.; Burriel, R.; Palacio, F.; Oliete, P. Synthesis, crystal structures, electronic structure and magnetic behavior of the trithiatriazapentalenyl radical, $C_2S_3N_3$. *J. Mater. Chem.* **2001**, *11*, 1992−2003.
(33) Brusso, J. L.; Clements, O. P.; Haddon, R. C.; Itkis, M. E.; Leitch, A. A.; Oakley, R. T.; Reed, R. W.; Richardson, J. F. Bistability and the phase transition in 1,3,2-dithiazolo[4,5-*b*]pyrazin-2-yl. *J. Am. Chem. Soc.* **2004**, *126*, 14692−14693.
(34) Bates, D.; Robertson, C. M.; Leitch, A. A.; Dube, P. A.; Oakley, R. T. Magnetic bistability in naphtho-1,3,2-dithiazolyl: solid state interconversion of a thiazyl π-radical and its N−N σ-bonded dimer. *J. Am. Chem. Soc.* **2018**, *140*, 3846−3849.
(35) Mills, M. B.; Wohlhauser, T.; Stein, B.; Verduyn, W. R.; Song, E.; Dechambenoit, P.; Rouzières, M.; Clérac, R.; Preuss, K. E. Magnetic bistability in crystalline organic radicals: the interplay of H-bonding, pancake bonding, and electrostatics in 4-(2′-benzimidazolyl)-1,2,3,5-dithiadiazolyl. *J. Am. Chem. Soc.* **2018**, *140*, 16904−16908.
(36) Shultz, D. A.; Fico, R. M., Jr.; Boyle, P. D.; Kampf, J. W. Observation of a hysteretic phase transition in a crystalline dinitroxide biradical that leads to magnetic bistability. *J. Am. Chem. Soc.* **2001**, *123*, 10403−10404.
(37) Itkis, M. E.; Chi, X.; Cordes, A. W.; Haddon, R. C. Magneto-opto-electronic bistability in a phenylenyl-based neutral radical. *Science* **2002**, *296*, 1443−1445.
(38) Peterson, J. P.; Zhang, R.; Winter, A. H. Effect of structure on the spin switching and magnetic bistability of solid-state aryl dicyanomethyl monoradicals and diradicals. *ACS Omega* **2019**, *4*, 13538−13542.
(39) Vela, S.; Reardon, M. B.; Jakobsche, C. E.; Turnbull, M. M.; Ribas-Arino, J.; Novoa, J. J. Bistability in organic magnetic materials: a comparative study of the key differences between hysteretic and non-hysteretic spin transitions in dithiazolyl radicals. *Chem. - Eur. J.* **2017**, *23*, 3479−3489.
(40) Venkataramani, S.; Jana, U.; Dommaschk, M.; Sönnichsen, F. D.; Tuczek, F.; Herges, R. Magnetic bistability of molecules in homogeneous solution at room temperature. *Science* **2011**, *331*, 445−448.
(41) Phan, H.; Lekin, K.; Winter, S. M.; Oakley, R. T.; Shatruk, M. Photoinduced solid state conversion of a radical σ-dimer to a π-radical pair. *J. Am. Chem. Soc.* **2013**, *135*, 15674−15677.
(42) Lekin, K.; Phan, H.; Winter, S. M.; Wong, J. W. L.; Leitch, A. A.; Laniel, D.; Yong, W. J.; Secco, R. A.; Tse, J. S.; Desgreniers, S.; Dube, P. A.; Shatruk, M.; Oakley, R. T. Heat, pressure and light-induced interconversion of bisdithiazolyl radicals and dimers. *J. Am. Chem. Soc.* **2014**, *136*, 8050−8062.
(43) Staveley, L. A. K. Phase transitions in plastic crystals. *Annu. Rev. Phys. Chem.* **1962**, *13*, 351−368.
(44) Ferrario, M. Orientational disorder and structural phase transitions in plastic molecular crystals. *NATO ASI Ser., Ser. E* **1991**, *205*, 381−393.

DOI: 10.1021/jacs.9b09533
J. Am. Chem. Soc. 2019, 141, 17989−17994

(45) Pouget, J.-P. The Peierls instability and charge density wave in one-dimensional electronic conductors. *C. R. Phys.* **2016**, *17*, 332−356.
(46) Emery, V. J. Basic ideas in the theory of organic conductors. *NATO ASI Ser., Ser. B* **1987**, *155*, 47−59.
(47) Agnew-Francis, K. A.; Williams, C. M. Catalysts containing the adamantane scaffold. *Adv. Synth. Catal.* **2016**, *358*, 675−700.
(48) Spilovska, K.; Zemek, F.; Korabecny, J.; Nepovimova, E.; Soukup, O.; Windisch, M.; Kuca, K. Adamantane - a lead structure for drugs in clinical practice. *Curr. Med. Chem.* **2016**, *23*, 3245−3266.
(49) Ciccotti, G.; Ferrario, M.; Memeo, E.; Meyer, M. Structural transition on cooling of plastic adamantane: a molecular-dynamics study. *Phys. Rev. Lett.* **1987**, *59*, 2574−2577.
(50) Amoureux, J. P.; Bee, M. Crystal structure of 1-cyanoadamantane, $C_{10}H_{15}CN$, in its plastic phase. *Acta Crystallogr., Sect. B: Struct. Crystallogr. Cryst. Chem.* **1979**, *B35*, 2957−2962.
(51) Me-AZADO is available commercially. For the preparation or properties of the radical, see, for example: Shibuya, M.; Tomizawa, M.; Suzuki, I.; Iwabuchi, Y. 2-Azaadamantane N-Oxyl (AZADO) and 1-Me-AZADO: highly efficient organocatalysts for oxidation of alcohols. *J. Am. Chem. Soc.* **2006**, *128*, 8412−8413.
(52) We could not achieve pressures above 900 bar because of dissolution of the sample in fluorinated oil, which was used as a pressure-transmitting medium.
(53) Matsumoto, S.; Higashiyama, T.; Akutsu, H.; Nakatsuji, S. A functional nitroxide radical displaying unique thermochromism and magnetic phase transition. *Angew. Chem., Int. Ed.* **2011**, *50*, 10879−10883.
(54) Nordman, C. E.; Schmitkons, D. L. Phase transition and crystal structures of adamantane. *Acta Crystallogr.* **1965**, *18*, 764−767.
(55) Bodach, A.; Fink, L.; Schmidt, M. U. Crystal structures of ordered and plastic-crystalline phases of iso-butyllithium by X-ray powder diffraction. *Chem. Commun.* **2018**, *54*, 10734−10737.
(56) Greer, S. M.; Oakley, R. T.; van Tol, J.; Shatruk, M.; Hill, S. Investigating the thermally- and light-induced interconversion of bisdithiazolyl radicals and dimers with high-field EPR. *Polyhedron* **2018**, *153*, 99−103.

DOI: 10.1021/jacs.9b09533
J. Am. Chem. Soc. 2019, 141, 17989−17994